

# Methods for Predicting Mechanical Deformations in the Breast During Clinical Breast Biopsy

F.S. Azar  
 U. of Pennsylvania  
 Dept. of BioEngineering  
 Philadelphia PA, 19104

D.N. Metaxas  
 U. of Pennsylvania  
 Dept. of Computer Science  
 Philadelphia PA, 19104

R.T. Miller  
 U. of Pennsylvania  
 Dept. of BioEngineering  
 Philadelphia PA, 19104

M.D. Schnall  
 U. of Penn Medical Center  
 Dept. of Radiology  
 Philadelphia PA, 19104

**Abstract** – A new method for clinical breast biopsy is presented, based on a deformable finite element model of the breast. The geometry of the model is constructed from MR data, and its mechanical properties are based on a non-linear material model. This method allows imaging the breast without compression before the procedure, then compressing the breast and using the finite element model to predict the tumor's position.

## I. INTRODUCTION

When doing high field (1.5T) magnetic resonance breast imaging, the use of a compression plate during imaging after a contrast-agent injection [1] may critically change the enhancement characteristics of the tumor, making the tracking of its boundaries very difficult. A new method for tracking the position of a hard inclusion in soft tissue is presented, based on a deformable finite element model (FEM) of the breast. The geometry of the model is constructed from MR data, and its mechanical properties are based on a non-linear material model. This method allows imaging the breast without compression before the procedure, then compressing the breast and using the finite element model to predict the tumor's position [2].

A deformable silicone gel phantom was built to study the movement of a stiff inclusion inside a deformable environment (as a tumor inside the breast) under plate compression. The phantom was imaged undeformed, then compressed. A 3D deformable model of the phantom was built from the resulting MR data using custom-written software (*BreastView*), and another FEM was built using a commercial pre-processor from the phantom's directly measured dimensions. The displacement vectors of the 8 corners of the stiff inclusion and its center were measured both from the MR images and from the two finite element models. The results suggest that the compressed model allows us to precisely track the position and motion of the stiff inclusion in the real compressed deformable environment.

## II. METHODS

### A. Phantom Construction

The phantom was designed to have magnetic properties (T1 and T2) similar to those of human breast tissue, to withstand large deformations (20% or greater), and to enable controlled deformations. The gel phantom was built using Sylgard Dielectric Gel 527 (Dow Corning, Midland, Mich.).

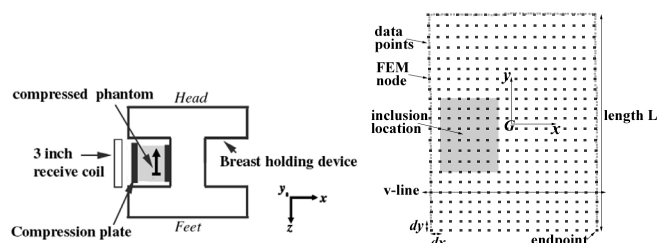


Fig. 1. Left: Top view of the setup for imaging the compressed gel phantom, Right: Construction of phantom model: 2D axial slice shown.

The geometry of the deformable phantom consists of a rectangular box (84x82x70mm) containing a rectangular inclusion (20x23x20mm), which is 4.3 times stiffer than the surrounding silicon.

### B. MR Imaging of Silicone Phantom

The full silicone gel phantom was placed in a custom-built pressure device, where a pressure plate could compress the gel phantom in a similar way as with a real breast with the desired amount of deformation (see Fig. 1). The whole setup was secured firmly and imaged with a whole body 1.5 T superconducting magnet (GE Medical Systems).

The silicone gel phantom was first imaged undeformed. The compression plate then applied a deformation width of 14% (9.8mm) in the x-direction, and the phantom was imaged again. An axial and a coronal T1-weighted fast multi planar gradient echo (FMPGR) sequences were performed in the uncompressed and compressed case.

### C. Material Properties of Silicone Phantom

The elastic properties of the phantom materials were evaluated on an Instron Model 1331 (Cambridge, MA) mechanical testing machine. Flat cylindrical samples of the silicone gel and the stiffer inclusion underwent uniaxial stress tests. Static load-deformation (stress-strain) curves were obtained. The silicone gel can be assumed to be an isotropic hyperelastic material (incompressible and temperature independent). The experimental data was fit the Mooney-Rivlin strain energy function [3]. By invoking the principle of virtual work, we derive the nominal stress-strain relationship:

$$T_v = 2 [1 - (1 + \epsilon_v)^{-3}] [(1 + \epsilon_v) \cdot C_{10} + C_{01}] \quad (1)$$

where  $T_v$  and  $\epsilon_v$  are the uniaxial nominal stress and strain respectively. Equation (1) was fit to the experimental stress-strain curves for the two types of silicone gel, using the least sum of squares method. The average parameter values calculated are  $C_{10} = 3740 \pm 64$  N/m<sup>2</sup>,  $C_{01} = 1970 \pm 34$  N/m<sup>2</sup> for

the surrounding silicone gel, and  $C_{10} = 16300 \pm 815$  N/m<sup>2</sup>,  $C_{01} = 10490 \pm 524$  N/m<sup>2</sup> for the silicone gel inclusion.

#### D. Geometric Model Construction

In order to create the 3D mesh, we first find the principal direction  $d$  (direction of the  $y$ -axis, Fig. 1), which for a real breast would be from the chest wall to the nipple. Any line with direction  $d$  in the plane of the contour, which intersects the contour, intersects it twice. This direction is that of the line orthogonal to the line which passes through the two endpoints. The center of gravity  $G$  of the contour set is calculated. The 3D mesh can now be easily generated following the  $U$  (along  $x$ ) and  $V$  (along  $y$ ) resolution desired, in the orthogonal  $(x,y)$  basis centered at  $G$ . This algorithm ensures that we have the same number of points on every  $V$ -line, and the same number of  $V$ -lines on every slice.

#### E. Deformable Phantom Models

The first model was built using the *BreastView* software [2]. The other model of the phantom was built directly from its physical dimensions using a pre-processor program MSC/PATRAN (MSC, CA), which automatically meshed the model. Both FEM's consist of 21 slices (each 4mm thick), stacked along the  $z$ -axis. The number of nodes in the  $x$ - and  $y$ -directions is 18 and 22 respectively, in order to have square shaped volume elements. The finite element models are made of 7497 elements each. The finite element modeling simulation was done using a robust finite element code Abaqus [4], commercially available.

Each element was modeled as a hybrid incompressible solid 8-node brick, which allows a fully incompressible constraint at each material calculation point [4]. The element material properties were given a homogeneous, isotropic, Mooney-Rivlin hyperelastic model, with the  $C_{10}$  and  $C_{01}$  constants as measured above. The boundary conditions were applied appropriately, and the 9.8mm displacement of the pressure plate was modeled in the initial conditions as a 9.8mm displacement constraint on every node, which belongs to the displaced surface of the phantom.

### III. RESULTS

The axial slice going through the center of the inclusion is shown in Fig. 2 in the uncompressed and in the compressed mode. A static displacement simulation was done with the *BreastView*-generated model. The simulation took ten full hours on an SGI workstation.

We tracked the displacement of the inclusion in the phantom. Using image analysis software, we measured the displacement vectors of the center of the inclusion, as well its eight corners. We used the axial slices to measure the  $x$  and  $y$  displacements, and the coronal slices to measure the  $z$  displacements. Table 1 shows the difference between the displacements from the *BreastView*-generated model, the PATRAN-generated model, and the experimental displacement results.

TABLE I  
DISPLACEMENT DIFFERENCES (MM) WITH THE *BREASTVIEW* MODEL  
DISPLACEMENT RESULTS, FOR EACH CORNER OF THE INCLUSION AND  
CENTER.

corner >	1	2	3	4	5	6	7	8	center	
x	PATRAN	0.0	0.0	0.0	0.0	0.0	0.1	0.1	-0.1	0.1
	experiment	0.5	0.3	0.3	0.4	0.2	0.4	0.4	0.2	0.4
y	PATRAN	-0.1	0.1	0.1	-0.1	-0.1	-0.1	-0.1	-0.1	-0.1
	experiment	0.7	0.3	-0.2	0.7	0.7	1.0	1.0	0.7	0.6
z	PATRAN	-0.2	0.0	-0.2	0.1	-0.5	-0.4	0.1	0.5	-0.2
	experiment	-0.7	-0.6	-0.1	0.1	0.0	0.6	-0.4	0.5	-0.6

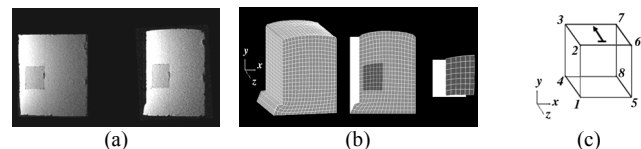


Fig. 2. (a) Uncompressed (left), and compressed (right) axial MR slice of phantom, (b) 3D view of model (left), axial slice through center of inclusion (middle), axial view of inclusion center (right), before and after compression, (c) Corner identification numbers for the stiff inclusion

The average errors in displacements were 0.34mm, 0.66mm, and 0.40mm in the  $x$ ,  $y$  and  $z$  directions respectively, and are within the maximum imaging error. The results show that the methodology used to create the phantom model using *BreastView* is sound since it results in a model, which yields virtually the same inclusion displacements as the PATRAN-generated model.

### IV. DISCUSSION

This initial phantom study shows that it may be possible to create a deformable model of the breast based on the use of finite elements with non-linear material properties capable of modeling the deformation of the breast. The geometry of the model is constructed from MR data, and the material properties of the different structures are computed independently using material testing techniques. The application of this deformable model to human breast data is currently underway.

This deformable model will be used as a new tool to the physician, who will: 1) image the breast with no compression (thus increasing the contrast and visibility of the tumor), 2) use the compression plates (to minimize deformations caused by the insertion of the needle), 3) compress the breast model, and accurately locate the tumor within the real compressed breast.

### REFERENCES

- [1] S. Heywang, A. Wolf, "MR imaging of the breast with Gd-DTPA: use and limitations", *Radiology*, vol. 171, pp. 95-103, 1989.
- [2] F. Azar, D. Metaxas, M. Schnall, "A finite element model of the breast for predicting mechanical deformations during interventional procedures", *Proc. ISMRM*, pp. 1084, 1999.
- [3] A. Green, W. Zerna, *Theoretical Elasticity*, Oxford U., pp. 99, 1968.
- [4] Hibbitt, Karlsson, Sorensen, *Abaqus/Standard ver. 5.8 Manual*, vol. II, pp. 14.1.4-1 to 14.1.4-17, 1998